Coriolis Flowmeter Verification via Embedded Modal Analysis *

Matthew Rensing**,** Research Engineer, Sheet Dynamics, Ltd., 1775 Mentor Ave. Mailbox Suite #227, Cincinnati, OH 45213 MRensing@sdltd.com

Timothy J. Cunningham, Principal Engineer, Micro Motion, Inc., 7070 Winchester Circle, Boulder, Colorado 80301 Tim.Cunningham@Emerson.com

NOMENCLATURE

ω: frequency radians/second
f: frequency Hz
$\delta\phi$: phase difference or delay radians
δt: time delay microseconds
FCF: flow calibration factor (gm/sec)/ microsec
$\dot{m}$: mass flow rate lbm/min
C: geometric constant, dimensionless
E: Young's modulus psi
I: beam moment of inertia in^4
L: length of flowtube in
H: frequency response function (FRF)

$\dot{x}$: velocity response in/sec
f: input force lbf
$v_{pickoff}$: pickoff voltage volts
i_{driver} : measured driver current amps
$i_{command}$: commanded driver current amps
R: residue
λ: pole
M, C, K: physical mass, damping, and stiffness

ABSTRACT

Verification of industrial flowmeters can be a costly endeavor, requiring significant factory downtime, but is often required to ensure measurement accuracy. A new feature, called Smart Meter Verification, now available on Coriolis meters uses embedded experimental modal analysis to confirm flowmeter accuracy. Smart Meter Verification has been successfully employed by numerous customers and has generated significant revenue. This paper outlines the evolution of this product from an offline, lab-based, concept to an embedded product. The embedded modal analysis fits a single degree of freedom model to the primary drive mode, based on frequency response measurements made at select tones near the drive mode. The estimated stiffness from each verification's modal analysis is compared to the stiffness from a factory baseline to ensure that the meter is still within calibration. Simultaneous multi-tonal excitation of the meter is used to maximize the usable signal generated from a limited excitation power budget, to cope with a time-varying system, and to minimize the complications of nonlinearity. MATLAB-based rapid software prototyping was used to prototype these embedded algorithms on a real-time DSP platform. Excitation of the flowmeter and measurement of response is performed using the transducers already on the device, and the model fit and control logic are performed using the existing embedded electronics. This has allowed the verification technique to be applied without changing the design of the flowmeter hardware.

INTRODUCTION

Experimental modal analysis typically is used as a tool for testing structures in the laboratory environment. These one-off lab tests can be used to confirm the dynamics of the structure or to correlate a structural model. Structural health monitoring goes a step further by performing ongoing testing and tracking the dynamics over time. Changes in the dynamics are used to indicate structural changes. In both of these approaches the structure is instrumented with transducers to measure the response and perhaps also to provide the excitation. These transducers, data acquisition systems, and analysis software are not necessary for the day to day operation of the structure. The tests usually require significant involvement of test personnel.

Micro Motion has developed a product called Smart Meter Verification that uses experimental modal and structural health monitoring techniques to ensure accurate measurement by its Coriolis mass flowmeters. The embedded digital signal processing (DSP), electronics, and transducers that are used to measure flow are multi-

tasked to perform ongoing modal analyses of the flowmeter structure. The modal results are tracked to provide assurances of the health of the meter. This new diagnostic has been a success in the marketplace.

The story of the development of Smart Meter Verification is an interesting case study. This paper will highlight some of the things that we learned in going from lab-based modal analysis to a reliable real-time product. We will first discuss the theory of operation of Coriolis flowmeters to get a background for the rest of the paper.

CORIOLIS FLOWMETER OPERATION

A Coriolis mass flowmeter directly measures the mass flow rate of a fluid by vibrating (driving) a fluid-conveying tube at resonance. Figure 1 shows a simplified "U" shaped tube geometry. Flow enters one leg of the tube and exits the other leg. The cross product of the moving fluid with the tube vibration develops Coriolis forces, as shown in Figure 1a., with F_C being the Coriolis force on the fluid and F_t being the equal and opposite force on the tube. The tube is commonly vibrated in a fundamental bending mode, Figure 1b.

A more realistic dual "U" tube flowmeter is shown in Figure 2. The flow enters from the pipeline and is split at an inlet manifold between the 2 U-shaped flowtubes. The flow is then rejoined at an exit manifold and continues down the pipeline. The tube vibrates in a balanced, out-of-phase fundamental bending mode, like a tuning fork. The Coriolis forces act on the tubes to perturb the vibrational motion, giving rise to a spatially varying phase angle along the tube as shown in the top view of Figure 2. The difference between phase angles at two or more two locations, which is called phase delay, is used to calculate mass flow rate.
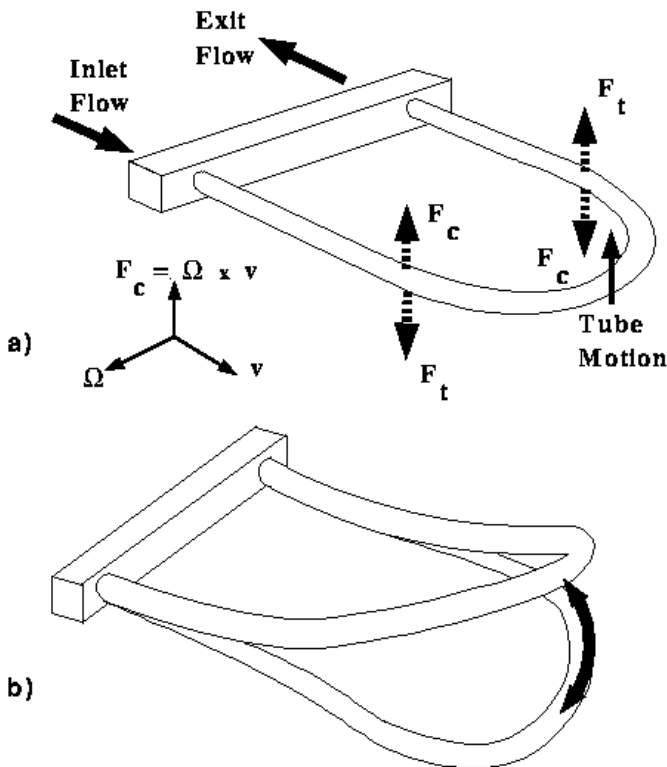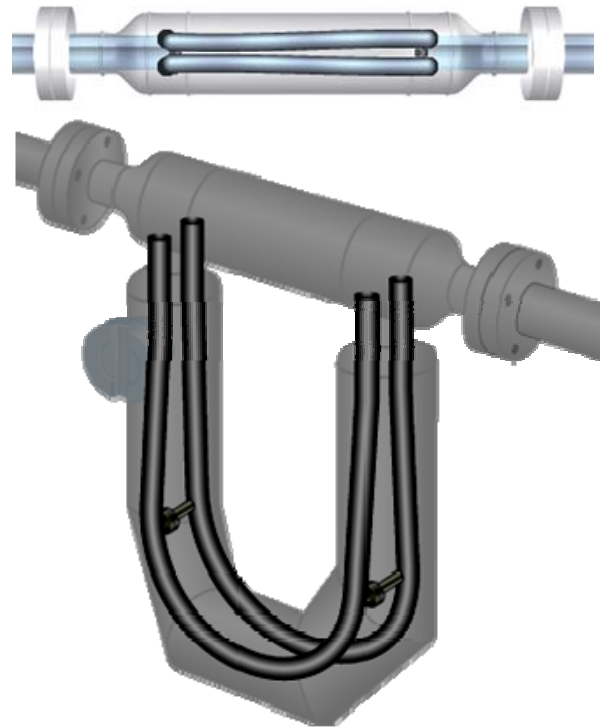

Figure 1. Coriolis Flowmeter Operation

Figure 2. Coriolis Mass Flowmeter

The mass flow rate calculation more commonly uses time delay (δt) rather than phase delay ($\delta\phi$). For a tube vibrating at resonance frequency ω, the two are related by Equation (1).

$$\delta t = \delta\phi / \omega \qquad (1)$$

The mass flow rate through a Coriolis sensor is directly proportional to this δt with the proportionality constant being the flow calibration factor (FCF) [1]. The mass flow rate through a sensor, $\dot{m}$, is given by

$$\dot{m} = FCF \cdot \delta t \qquad (2)$$

FCF therefore is defined in units of mass flow rate/time delay. A typical set of units for FCF is (gm/sec)/μsecond.

The transducers used to measure flow (called "pickoffs") are voice coil velocity transducers, with the magnet mounted on one tube and the coil on the other tube, as shown in Figure 2. These transducers produce a voltage proportional to the tube velocity. Since the tube is vibrating at resonance the voltage is sinusoidal. The flowmeter's DSP based electronics process the pickoff voltages to measure flow.

Not shown in the figure is the driver transducer, another voice coil. Sinusoidal current is applied to the coil, which, in conjunction with the magnet, produces equal and opposite forces on the flow tubes. The electronics also use the pickoff signals in a closed-loop control scheme to maintain the resonant frequency at a set amplitude.

CORIOLIS FLOWMETER VERIFICATION

Coriolis flowmeters contain no moving parts and typically last for 10 or more years. They are also unique among flow measurement devices in that the mass flow measurement is unaffected by the process fluids; that is, the flow calibration factor (FCF) is unchanged over the life of the flowmeter. However in many applications, such as custody transfer where the flowmeter is used essentially as a cash register or the pharmaceutical industry where processes need to be tracked rigorously, a method of verifying the accuracy of the flowmeter is highly desirable.

Micro Motion's original electronics were of course analog, being developed in the 1980s. Their diagnostic capabilities were extremely limited. Micro Motion introduced digital signal processing into their attached electronics in 2002. DSP allowed us to expand our diagnostic capabilities. When we were developing the next generation DSP-based electronics, an embedded self diagnostic was a key requirement. With our understanding of the structural dynamics of the flowmeter we felt we could develop this diagnostic.

MODAL ANALYSIS AND CORIOLIS FLOWMETERS BACKGROUND

Micro Motion first started using experimental modal analysis in the late '80s to improve the product development process. At about the same time we adopted finite element analysis. Initially experimental modal analysis was used to verify the frequencies of its flowmeters. Modal analysis was later used to correlate finite element models to achieve better modeling fidelity. These modal analyses were done in the typical manner in that a test specimen was instrumented in the lab and, in our case, impact tested. Modal parameters and mode shapes were extracted from the experimental data. The data was correlated to finite element models which we used to improve our modeling techniques.

Experimental modal testing done in this way had its downsides. First, the experimental setup, acquisition, and analysis were time-consuming. Gaining access to test points on the flowmeter required modifications of the standard production units, specifically cutting holes in the case, which needed special tooling and changed the dynamics of the sensor. Adding the accelerometers mass-loaded the structure significantly, which also changed the dynamics.

To improve the modal data acquisition, Micro Motion took advantage of the driver and pickoffs, normally used to drive the tubes and measure flow, for the modal analysis actuation and response. These transducers eliminated the need to cut access holes in our meters and eliminated any additional mass loading or damping caused by attaching accelerometers. Modal analyses using burst random excitation into the driver and standard data acquisition with a signal analyzer gave us very good results. With this significant improvement in modal results, and improved FE models, we developed new insight relating the modal results to the flow measurement.

MODAL THEORY LEADS TO BREAKTHROUGH DIAGNOSTIC

A key breakthrough in Micro Motion's Smart Meter Verification product started with recognizing that the flow calibration factor is directly related to the tube stiffness. Equation (2) can be derived from first principles, for example starting with the Housner differential equation describing a fluid-conveying beam [2, 3]. These derivations result in a term corresponding to the FCF as shown in Equation (3).

$$\dot{m} = C \frac{EI}{L^3} \cdot \delta t \qquad (3)$$

where C is a dimensionless geometric constant related to the boundary conditions and beam properties. The EI/L^3 term, corresponding to the FCF, has units of force/length, the units of stiffness.

Going through these derivations in detail to show this relationship between stiffness and flow calibration factor is beyond the scope of this paper. However a much simpler dimensional analysis also shows that the FCF is related to stiffness by showing that they have the same units. Rearranging Equation (2)

$$FCF = \frac{\dot{m}}{\delta t} \qquad (4)$$

shows that the units of the FCF are mass flow rate/time delay. The FCF is shown dimensionally as

$$\frac{\left(\dfrac{Mass}{Time}\right)}{Time} \qquad (5)$$

For example, FCF is commonly expressed in units of (gm/sec)/μsec. In a consistent system of units, mass can be represented by force/(acceleration of gravity), taking advantage of Newton's Second Law. Plugging this into equation (5) shows that the flow calibration factor has units of stiffness, (Force/Length).

$$\frac{\left(\dfrac{Mass}{Time}\right)}{Time} = \frac{\left(\dfrac{Force * Time^2 / Length}{Time}\right)}{Time} = \frac{Force}{Length} \qquad (6)$$

With this understanding the stage was set to use the modal analysis derived stiffness as a calibration diagnostic. Developing the capability to do these modal analyses in real time was necessary to implement this diagnostic.

RAPID PROTOTYPING WITH MATLAB/SIMULINK/REATIMEWORKSHOP/DSPACE

In the mid-90s Micro Motion started to investigate the use of modal filters to improve its digital signal processing. These modal filters required extremely accurate modal parameters, with the mode shape coefficients extracted from the driver and pickoff transducers. These modal analyses taxed our standard signal analyzers in terms of data storage and programming flexibility.

To improve our data acquisition and modal analysis capabilities we acquired a dSPACE rapid prototyping system. The dSPACE system leverages Matlab core numerical routines and Simulink's graphical signal processing capabilities. Signal flow diagrams implemented in Simulink can be converted into real-time executable code for the dSPACE processor. dSPACE has A/D and D/A I/O blocks for Simulink to handle the transducer I/O.

We implemented our techniques for performing modal analysis using the onboard transducers via the rapid prototyping system. This modal approach required files larger than 100 MB taking approximately 20 minutes of data collection to obtain the required frequency resolution to extract the modal parameters of interest. Extracting the modal parameters was a manual process requiring engineering judgment and a fair amount of time for each iteration. However, the modal parameters were precise enough that we could correlate them to the FCF. We decided that if we could embed this modal analysis we would have a viable diagnostic product.

DEVELOPMENT OF EMBEDDED METER VERIFICATION

Micro Motion had shown that it could extract good stiffness measurements using the onboard transducers in a time consuming, off-line measurement process. The challenge was being able to implement that measurement process into an extremely robust one operating in an embedded environment. Our initial development was done using a dSPACE rapid prototyping system connected to the meter's transducers, but techniques were developed with an eye toward implementation in the embedded hardware that is an inherent part of the flowmeter. For customers to benefit from this verification process it had to be simple to use, with minimal user interaction. This meant no additional instrumentation would be required, no additional processing hardware would be connected, and minimal restrictions would be placed on the user's process. The embedded implementation of Meter Verification would have to run on the existing processing platform and use the existing transducers already on the meter. These restrictions provided significant challenges beyond the initial laboratory proof-of-concept – the sections below lay out how we addressed some of these challenges.

TRANSDUCERS AND ELECTRONICS

The meters on which the verification algorithm was developed employ a single driver for input and two pickoffs for output (with phase measured between the two pickoffs – see Figure 2). Using these as inputs and outputs for verification means that we used a single-input multiple-output (SIMO) system model (the model is explored in more detail below). Using the same transducers and electronics to measure flow and to perform meter verification enhances the correlation between the measured meter stiffness and the flow calibration factor. Both the driver and pickoffs are voice coil devices, converting current to force as a driver, and velocity to voltage as a pickoff. Since the pickoff measurements are in terms of velocity, our model was formulated in terms of velocity.

The transducers do suffer from some limitations as compared to laboratory-grade instruments (e.g. accelerometers). The primary limitation of the transducers is a mild nonlinearity; the calibration of the transducers is a function of the instantaneous engagement (i.e. the position of the permanent magnet relative to the wire coil, which is simply the distance between the flow tubes), and is also affected by the rotational component of tube vibration (the alignment of the coil and the magnetic field changes when the flow tubes are not perfectly parallel). Another limitation of the transducers is their temperature dependence; the calibration of the transducers changes slightly with temperature, but this effect becomes significant given the large range in allowed operating conditions for the meters and the sensitivity of the stiffness measurement.

The electronics used in the embedded processing platform also provided challenging limitations. Only two high-speed analog to digital converters were available on the board, limiting the number of system parameters that could be simultaneously measured. The embedded processor itself was a fixed-point device, with limited compute cycles and system memory available. Finally, the current amplifier used to drive the excitation had limited output current available. We addressed these limitations imposed by the electronics and transducers in a number of ways, as described below.

EXCITATION

With copious off-line computing resources available, burst random excitation was a viable approach. However, this technique was inappropriate for an embedded approach. In order to maintain a flow measurement during verification, we had to maintain the closed-loop excitation of the fundamental bending mode with minimal interference from other excitations. The limited excitation power available also weighed against a burst random excitation.

The first excitation technique we considered as an embeddable replacement for the burst random approach was a sinusoidal excitation at a second frequency near the resonance frequency. The method would generate a frequency response function by measuring the excitation and response at the non-drive frequency, stepping the excitation sequentially among four frequencies near the drive. The FRF coefficients measured at these frequencies (plus the FRF coefficient for the drive frequency) would be used as inputs to the model fit. Ultimately, this approach proved unsatisfactory on several counts. The measurement was quite time consuming; the digital filtering then in use to resolve the narrow frequency bands required a few minutes to settle when conditions changed, pushing the total measurement time near 10 minutes. This long measurement time, while undesirable, was not in and of itself a dealbreaker. However, the fact that the system was not perfectly stationary over this time frame was a problem. Small changes in temperature and/or fluid density meant that the FRF coefficients at different frequencies were taken from slightly different systems. These differences required normalizing the data for the curve fit, increasing the computational difficulty and increasing the variability of the results.

We had much better success by simultaneously applying and measuring responses to the four "test" frequencies near the resonance (in addition to the ongoing resonance excitation). This had some drawbacks (increased computational load to simultaneously measure FRF coefficients at 5 frequencies, having to divide the excitation power budget amongst all the tones) but the benefits of making simultaneous measurements of the same system greatly outweighed these problems. The additional tones were generated open-loop at fixed frequencies and added to the closed-loop excitation of the resonance. Determining the exact frequencies for the additional tones involved balancing several concerns. Our desire to maximize the response amplitude (for signal-to-noise purposes) results in tones closely clustered near the lightly-damped resonance, but tightly spaced tones require additional time and tighter filtering to resolve. Much consideration went into determining the optimal spacing of these additional test tones, the results of which we consider proprietary. Figure 3 shows a typical frequency response function curve with four test tones and the drive tone indicated.

A few practical issues associated with the excitation arose that we had to deal with. The first problem was that the additional test tones influenced the closed-loop excitation of the resonance, which sought to keep the drive amplitude constant. This affected the stability of the closed-loop control and influenced the ongoing flow measurement. We handled this by simply digitally filtering out the known test frequencies from the pickoff signals that are fed back to the closed-loop controller (after the FRF coefficients are measured), using tightly designed and phase-adjusted notch filters. Other problems included working within the available power budget for excitation and minimizing nonlinear effects from the transducers. Both of these were addressed by reducing the amplitude of the closed-loop resonance drive. During normal operation a large amplitude excitation was used to produce a good phase measurement to determine flow; during meter verification, though, we used a lower amplitude at the

Figure 3. FRF Estimation

resonance to free up drive current to be distributed amongst the additional test tones (which required more input force to achieve reasonable response levels). The lower overall motion of the meter also dramatically reduced the nonlinear behavior of the transducers.
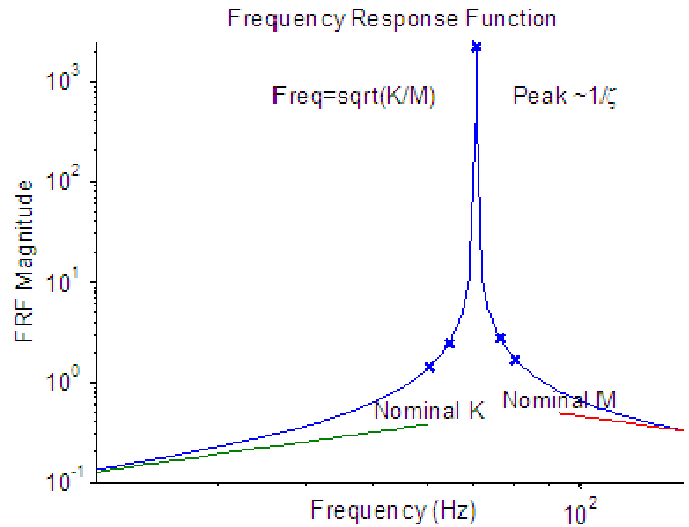
A final issue we encountered with the excitation is that the sudden application of the four test tones could act as an impulsive shock to the system. This impulse upset the closed-loop drive and took some time to die out in our lightly damped system. For this reason the test tones had to be started out at low amplitude and slowly ramped up to full power. This ramping extended the total measurement time somewhat, but ultimately proved faster than waiting for impulses to the meter to decay.

AMPLIFIER CALIBRATION

At its core the meter verification algorithm fitted a model to FRF coefficients measured at select frequencies. These FRF coefficients were defined as:

$$H \equiv \frac{\dot{x}}{f} \approx \frac{v_{pickoff}}{i_{driver}} \qquad (7)$$

With two pickoffs and a single driver, we had to measure three quantities to compute the FRF coefficients. However, as outlined above, only two high-speed A/D channels were available on the embedded hardware. To address this we split the measurement process into two steps. First, the current amplifier was calibrated by computing an FRF of the commanded current to the measured current. Then the pickoff responses were measured with respect to the commanded current. We'd then combine the two responses to produce the desired system FRF defined in Equation (7):

$$H \approx \frac{v_{pickoff}}{i_{driver}} = \frac{v_{pickoff}}{i_{command}} \frac{i_{command}}{i_{driver}} \qquad (8)$$

We used a hardware switch to toggle between feeding the measured current or a pickoff response into one of the A/D converters. The fact that pickoff and commanded current measurements were now taken at two points in time may seem to be an issue, but this was not problematic in the way that measuring at sequential frequencies had been. This was because the current amplifier is much more time-invariant than the meter itself. The amplifier calibration was performed immediately before the system FRFs were computed, and was measured driving at the same amplitude and frequencies as were used for the system FRFs. The only expected short-term causes of change in the amplifier's behavior were temperature changes or saturation of the amplifier (i.e. requiring more current or voltage than the hardware can supply). Saturation is unlikely to be an issue, since calibration was done under the same conditions as the measurement. Since the electronics are not thermally coupled to the flow

tubes, temperature changes were not likely to affect the amplifier either. In any case, temperature effects were less pronounced on the current amplifier than on the flowmeter itself. While this amplifier calibration process did add some time to the total measurement and briefly interrupt the measurement of flow, it did effectively cope with the limited capabilities of the embedded hardware.

FRF MEASUREMENT

FRF coefficients were measured for the two pickoffs at the five excited frequencies (the resonant frequency and the four test tones). Since the excitations were tonal we computed the FRF coefficients by separately demodulating and filtering each tone, rather than any sort of Fourier-based approach. In this way we avoided leakage effects and reduced the amount of processing required. Still, the filtering required was somewhat taxing. To minimize the required processing and speed the transient response time we used a multi-stage filtering approach. The filters for each stage were carefully designed to minimize the filter order. The final filter stage had to provide a lowpass cutoff sharp enough to ensure that none of the other tones interfered (effectively forming a frequency band around each tone). Once we separated the input and output signals by frequency using this demodulation and filtering we applied H_1 FRF average:

$$H = \frac{\dot{x} \cdot f^H}{f \cdot f^H} \qquad (9)$$

An H_1 FRF technique attempts to minimize noise on the output measurement and assumes the input measurement is comparatively clean [4]. 25 averages were used in computing each FRF coefficient; with the decimation already applied to the input and output signals, this resulted in a set of FRF coefficients once every 5 seconds. Along with the FRF coefficients we also calculated the coherence. This was generally quite excellent (at least 0.99999), and can be attributed to the excellent SNR of the tonal excitations and the tightly filtered signal processing.

At this point we also addressed the temperature dependence of the transducers. A flowtube temperature measurement was already in place for compensating the flow and density measurements. This temperature measurement was combined with the known temperature dependence of the transducers to rescale the FRF coefficients back to the measurements that would have been made at a nominal temperature.

MODEL FITTING

With the FRF coefficients measured, several different forms of a second-order dynamics model could be fit to estimate the modal parameters. We ultimately selected a single DOF pole-residue model for this algorithm after testing was done with several other candidate forms. The starting point for the pole-residue model (which is based on a velocity rather than position output variable) was of the form

$$H(\omega) = \frac{R \cdot j\omega}{j\omega - \lambda} + \frac{\bar{R} \cdot j\omega}{j\omega - \bar{\lambda}} \qquad (10)$$

Figure 4. Pole Residue Model Compared to 2nd order System

The pole λ and the residue R are both complex-valued. The second term of Equation (10), corresponding to the negative frequency half of the response, was then dropped. As demonstrated in Figure 4, the elimination of the negative frequency contribution has a negligible effect near the positive-frequency resonance. We preferred this form over a full second-order system model to better fit the limited resources available on the embedded hardware.
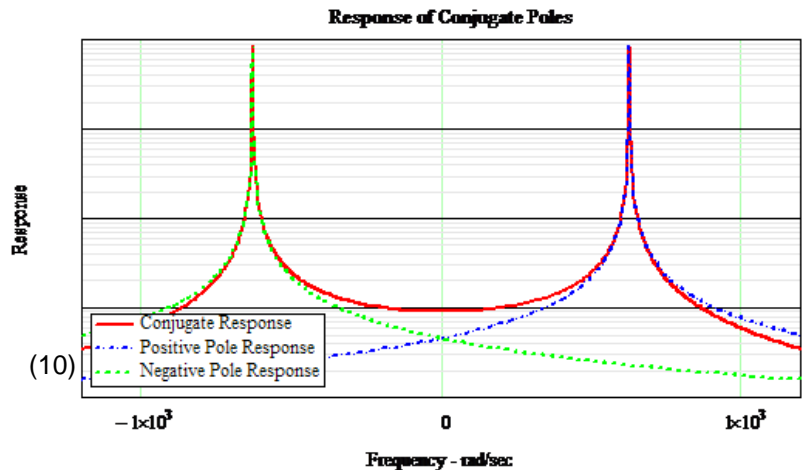
We then extended the basic pole-residue model to accommodate the two-output system by fitting two residues and a single pole to the FRFs, since the pole of the system is independent of the measurement location. This system of equations is shown in Equation (11). Note that the equations are dependent on the frequency. The system of equations is expanded for each of the 5 frequencies measured, producing an overdetermined system with 10 complex equations and 3 complex unknowns.

$$
\begin{bmatrix} 1 & 0 & \dfrac{H_L(\omega)}{j\omega} \\[2mm] 0 & 1 & \dfrac{H_R(\omega)}{j\omega} \end{bmatrix} \cdot \begin{bmatrix} R_L \\ R_R \\ \lambda \end{bmatrix} = \begin{bmatrix} H_L(\omega) \\ H_R(\omega) \end{bmatrix} \tag{11}
$$

Solving this overdetermined system of equations (in the least-squares sense) is simple in, say, MATLAB, but requires some thought in an embedded system. We chose to first simplify the complex pseudo-inverse into a real inverse, then solve with standard matrix techniques and software emulation of floating-point math (the processing load in doing so was tolerable, since the model was fit only once per 5 seconds). The simplification, starting from a generic system of equations $Ax = b$, is performed as

$$
\begin{aligned}
Ax &= b \\
A^H A x &= A^H b \\
x &= \left(A^H A \right)^{-1} A^H b
\end{aligned} \tag{12}
$$

Note that $A^H A$ is a strictly real 3x3 matrix whose inverse can be easily found.

EXTRACTING SYSTEM PARAMETERS

As discussed earlier, our primary goal with meter verification was to measure the meter stiffness, monitoring for changes that may indicate a flow calibration factor change. Obtaining stiffness and other physically-meaningful system parameters from the pole-residue model was straightforward, and can be derived by equating the system of Equation (10) to an MCK model,

$$
H = \frac{j\omega}{-M\omega^2 + jC\omega + K} \tag{13}
$$

Since the stiffness is compared to a baseline stiffness, though, we found it necessary to compensate for any *expected* changes to the stiffness. Micro Motion has long compensated for the change in tube stiffness as a function of temperature, using experimentally-derived coefficients for the change in Young's modulus as a function of temperature. These correction coefficients were applied in conjunction with the measured tube temperature to the stiffness derived from the pole-residue model, correcting it back to the equivalent stiffness at a nominal temperature.

The calculations used to extract stiffness and other quantities from the pole-residue model are shown in Figure 5. This graphical representation was taken from the rapid prototyping environment used to initially develop the algorithms, and comprised only one of the many subsystems associated with implementing the algorithm. Throughout the development process we made extensive use of this rapid prototyping framework. The graphical signal-flow approach made it easy to rapidly change techniques, debug problems, and try new ideas. Only after the final form of the algorithm was determined did we go about hand-writing code for the embedded platform, using the rapid prototyping diagrams as the reference for the implementation.

PRESENTATION OF STIFFNESS RESULTS TO THE CUSTOMER

Presenting diagnostic results to customers is a very involved topic. This paper will just discuss briefly how we present the stiffness as a Meter Verification diagnostic using the deviation from a factory baseline.
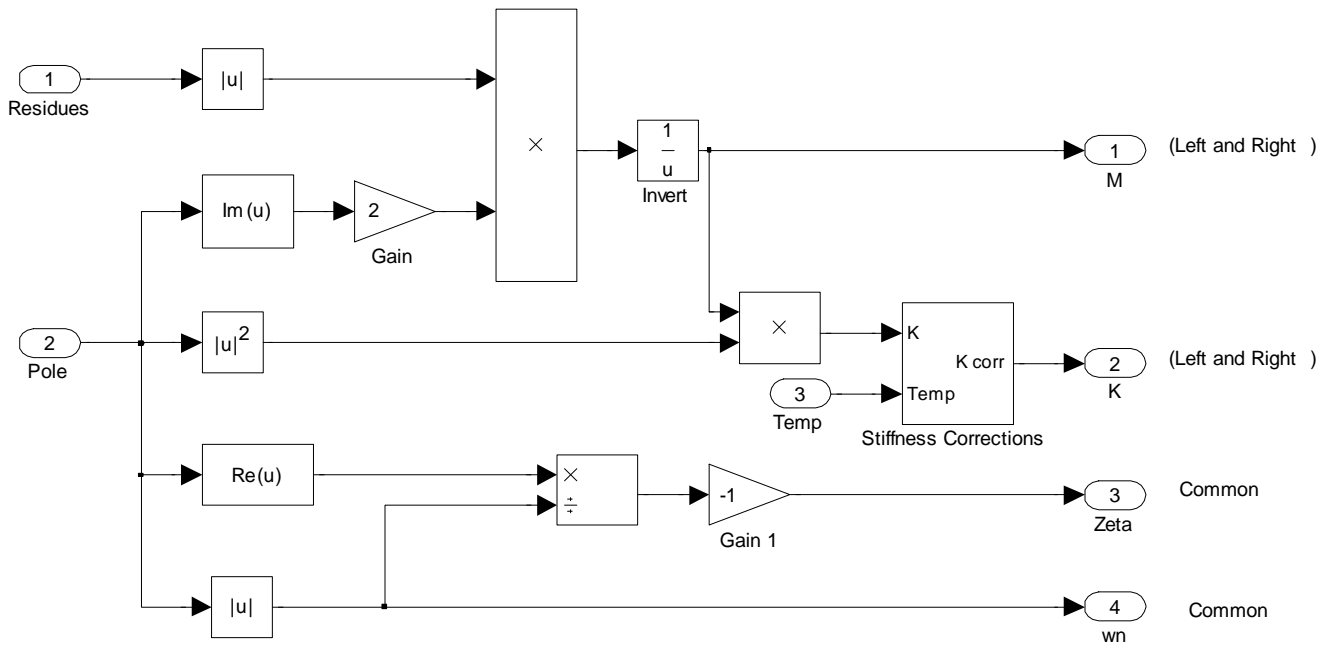
Figure 5 – Variable extraction as implemented in Simulink/dSPACE rapid prototyping environment

During the standard calibration of the flowmeter, a factory baseline stiffness is calculated and stored in the transmitter. Customer initiated verifications are normalized as a percent deviation from the factory baseline, which we define as the stiffness uncertainty. The stiffness uncertainty normalization is shown below.

$$stiffness_{uncertainty} = \left(\frac{stiffness_{measured}}{stiffness_{factory\ baseline}} - 1 \right)\% \qquad (14)$$

The standard deviation of the stiffness uncertainty is much better than the baseline accuracy of the flowmeter, as shown in Figure 6. Under lab conditions this deviation is on the order of 0.01%. While many field effects are compensated for, there can be residual uncompensated error in the stiffness uncertainty. The spec limits for the stiffness uncertainty has been set to account for these potential residual errors. Over the entire range of process conditions, temperature, pressure, flow rate, density, etc. there is less than a 0.3% (3σ) chance of a false alarm (i.e. indicating that the sensor has changed when it hasn't). The meter verification diagnostic results are discussed more thoroughly in the references [5, 6, 7]
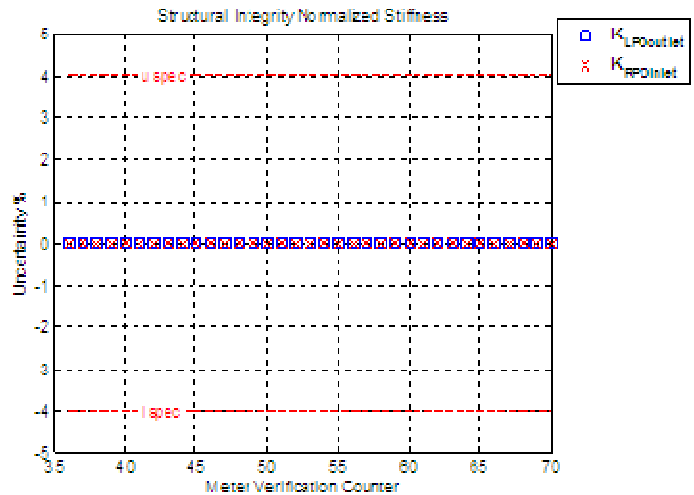

Figure 6. Presentation of Meter Verification Results

CONCLUSION

Micro Motion Smart Meter Verification embeds experimental modal analysis in an industrial device. Data acquisition, control, and the modal parameter estimation process have been automated to produce the desired physical estimates of the model parameters. The stiffness estimate that comes out of the modal analysis provides an independent estimate of the flowmeter calibration.

Embedding a modal analysis required a significant amount of development work to overcome the constraints of the embedded hardware. The embedding efforts were greatly aided by the use of a DSP rapid prototyping system.

Smart Meter Verification is extremely robust and provides customers with a diagnostic that ensures that their Coriolis flowmeter is operating at the specified factory accuracy. Micro Motion has been able to meet a significant customer need by embedding modal analysis into a successful product.

REFERENCES

[1] Micro Motion TUTOR, http://www.emersonprocess.com/micromotion/tutor/index.html.

[2] Lange U., Levien A., Pankratz T., Raszillier H., *Effect of detector masses on calibration of Coriolis flowmeters,* Flow Measurement Instrumentation, Volume 5 Number 4, 1994.

[3] Stack C., Garnett R., Pawlas G., *A Finite Element for the Vibration Analysis of a Fluid-conveying Timoshenko Beam*, 34th SDM conference proceedings, 1993, AIAA

[4] Brown, D., Allemang, R., Phillips, A., *Structural Measurement Lecture Notes*, UC-SDRL Experimental Techniques Seminar Series, Chapter 6. 2004.

[5] Cunningham T., Stack C., Connor C., *Using Structural Integrity Meter Verification*, Micro Motion White Paper WP-00948, www.micromotion.com, 2007.

[6] Cunningham T., *Using Structural Integrity Meter Verification to Track Corrosion in Coriolis Flowmeters*, Micro Motion White Paper WP-01196, www.micromotion.com, 2009.

[7] Cunningham, T., *An IN-SITU Verification Technology for Coriolis Flowmeters*, Proceedings of the 7th International Symposium on Fluid Flow Measurement, 2009.